

Robustness of topologically sensitive harmonic generation in laser-driven linear chains

Helena Drüeke and Dieter Bauer

Institute of Physics, University of Rostock, 18051 Rostock, Germany

(Dated: May 3, 2019)

A many-order-of-magnitude difference in the harmonic yield from the two topological phases of finite, dimerizing linear chains in laser fields has recently been observed in all-electron time-dependent density functional simulations [D. Bauer, K. K. Hansen, Phys. Rev. Lett. **120**, 177401 (2018)]. In this work, we explore the robustness of the effect concerning the length of the chains, a continuous transition between the two topological phases, and disorder. A high robustness of both the degeneracy of the edge states in the topologically non-trivial phase as well as of the pronounced destructive interference, causing a dip in the harmonic spectra, in the topologically trivial phase is observed.

I. INTRODUCTION

The exploration of the territory between strong-field short-pulse laser and condensed matter physics has only recently gained momentum. Electron dynamics [1–4] and high harmonic generation [5–13] are studied in crystals as well as amorphous solids [14]. Studies on noble gases allow for comparison of high harmonics produced by gases and their corresponding solids [15]. Furthermore, first investigations on two-dimensional solids, such as monolayer graphene [16–18] or ferromagnetic monolayers [19] are being performed.

High harmonic generation in gases can be explained by the three-step-model [20, 21]. In the first step, an electron tunnels into the continuum. The electron is then accelerated by the oscillatory laser field in the second step and possibly driven back to its parent ion. In the third step, the electron may recombine with the ion upon emission of high-harmonic radiation. The three-step-model can be adapted for solids by taking the band structure into account. The atomic ground state is replaced by the valence band, the continuum by the conduction bands, and the recombination of the electron with its parent ion by the recombination of the electron moving in one of the conduction bands with the hole moving in the valence band [22]. This so-called interband harmonic generation can well explain the cut-offs observed in ab-initio simulations (see, e.g., [23, 24]). Intraband harmonics, on the other hand, are caused by electrons moving within bands. Due to the varying curvature of the bands, this motion generates harmonics as well. These harmonics are expected to be dominant for harmonic energies below the band gap between the lowest (laser-dressed) conduction band and the valence band because the three-step mechanism does not generate such sub-band-gap harmonics. One might expect that a fully occupied valence band does not produce intraband harmonics. However, in a simulation with non-interacting (Kohn-Sham) electrons, all electrons move and, individually, generate harmonics. It is only by destructive interference that the total harmonic yield largely cancels.

One of the fascinating research directions in condensed matter physics, cold atoms, and photonics are topological phases with interesting properties, and transitions

between them [25]. From the strong-field laser perspective, there are only very few investigations on that subject to date [26–30]. Many questions arise in that context, for instance: How are topological phases encoded in typical strong-field observables such as photoelectron or harmonic spectra? How can strong, short-pulse lasers be used to manipulate topological phases? May topological edge states be useful to develop ultrafast, light-driven electronic devices or, vice versa, electronically driven, novel light sources? And from the theoretical perspective: Is the usual tight-binding modeling enough to properly describe the nonlinear light-matter interaction? Which are the suitable and useful topological invariants? Does the laser need to illuminate the edges to have topological edge effects in photoelectron or harmonic spectra?

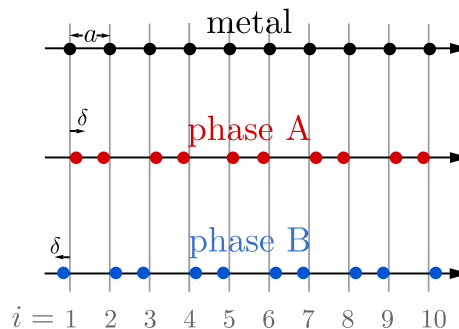


FIG. 1. Sketch of the ion positions for a dimerizing chain of length $N = 10$: equidistant separations a (metal), ions shifted alternately to the right and the left ($\delta > 0$, phase A), ions shifted alternately to the left and to the right ($\delta < 0$, phase B).

In Ref. [28], a many-order-of-magnitude different harmonic yield is observed in the sub-band gap regime for the two topological phases of dimerizing linear chains. Figure 1 illustrates the setup. A linear chain of equidistantly separated atoms with one electron per atom has a half-filled valence band and thus is a metal. By shifting the atoms by δ alternately to the left and to the right (or vice versa), pairs of atoms with a shorter distance $a - |\delta|$ between each other are formed. In the band structure, a gap opens, the total energy decreases (Peierls instability), and the system becomes insulating. How-

ever, in so-called phase A all atoms are paired whereas in phase B the two edge atoms remain unpaired. This difference may look trivial at first but has profound consequences, which are most clearly elucidated using the Su-Schrieffer-Heeger (SSH) model [31, 32]. The SSH model is a tight-binding version of the situation depicted in Fig. 1: electrons hop with higher probability between the paired sites and with lower probability between the more distant sites. The SSH model for the bulk is simple enough to allow for the definition of a winding number as a topological invariant. It turns out that phase A is topologically trivial while phase B has a non-vanishing winding number [32]. The simulations in Ref. [28] are based on time-dependent density functional theory (TDDFT) [33, 34], which goes far beyond a tight-binding, independent-electron treatment. Nevertheless, the main topological feature of the SSH model—the presence of degenerate topological edge states—is “inherited” by the less idealized TDDFT description. The difference in the harmonic yield (also seen in Fig. 4 below) is attributed to pronounced destructive interference of all the electrons’ intraband harmonic emission from the valence band of the topologically trivial phase A while the destructive interference is spoiled by the presence of half-occupied edge states in the topologically non-trivial phase B (with edge ions).

From a practical point of view, robustness is the most appealing asset of topological matter because of potential applications, for instance in quantum computation (topological qubits [35]) or high-temperature superconductivity [36]. In the present paper, we investigate the robustness of the topological effect in harmonic generation observed in [28] with respect to chain size, continuous phase transition, and disorder.

The paper is organized as follows: We review the TDDFT model in Section II. The robustness of the degeneracy of the edge states and the harmonic spectra is investigated in Section III with regard to size dependence (subsection III A), a continuous phase transition (subsection III B), and disorder in the ion positions and ion potentials (subsections III C and III D, respectively). We summarize in Section IV.

Throughout this paper, atomic units $\hbar = |e| = m_e = 4\pi\epsilon_0 = 1$ are used unless stated otherwise.

II. DENSITY-FUNCTIONAL MODEL FOR LINEAR CHAINS

The model system used in this work is the same as in [28], a linear chain of N singly charged ions. Starting from an equidistant spacing, the ions are alternately shifted by δ to the left and to the right (see Fig. 1), leading to ion positions

$$x_i = \left(i - \frac{N+1}{2}\right)a - (-1)^i\delta, \quad i = 1, 2, \dots, N \quad (1)$$

with the lattice constant a and shift δ . The interaction of an electron (at position x) with the ions is described by the sum of the soft-core Coulomb potentials

$$v_{\text{ions}}(x) = \sum_{i=1}^N v_i(x) = - \sum_{i=1}^N \frac{1}{\sqrt{(x-x_i)^2 + \varepsilon_i}}. \quad (2)$$

We choose the same smoothing parameter for all ions, $\varepsilon_i = 1$, except for subsection III D, where topological robustness with respect to random fluctuations of the ε_i is investigated.

We use time-dependent density functional theory [33, 34] to calculate the electronic states of the system and its dynamics in the laser field. The time-dependent Kohn-Sham potential

$$v_{\text{KS}}[n](x, t) = v_{\text{ext}}(x, t) + u[n](x, t) + v_{\text{xc}}[n](x, t) \quad (3)$$

is the sum of the external potential $v_{\text{ext}}(x, t)$, the Hartree potential $u[n](x, t) = \int n(x', t)/\sqrt{(x-x')^2 + 1} dx'$, where $n(x, t)$ is the electron density, and the exchange-correlation potential $v_{\text{xc}}[n]$. The topological effects studied in the present work are robust with respect to the choice of $v_{\text{xc}}[n]$, therefore we use the simple adiabatic exchange-only local density approximation $v_{\text{xc}}[n] \simeq -[3n(x, t)/\pi]^{1/3}$. The external potential $v_{\text{ext}}(x, t) = v_{\text{ions}}(x) - iA(t)\frac{\partial}{\partial x}$ consists of the ionic potential $v_{\text{ions}}(x)$ and the coupling to the laser field described by the vector potential $A(t)$ in velocity gauge and dipole approximation (with the A^2 -term transformed away).

The implementation consists of two parts: First, imaginary-time propagation is used to self-consistently determine the occupied (and, if of interest, unoccupied) Kohn-Sham orbitals φ_i without an external driver. In the second part, the influence of a laser pulse on the orbitals is simulated using real-time propagation. The orbitals are propagated according to the time-dependent Kohn-Sham equation

$$i\partial_t\varphi_i(x, t) = \left[-\frac{1}{2}\frac{\partial^2}{\partial x^2} + v_{\text{KS}}[n](x, t)\right]\varphi_i(x, t) \quad (4)$$

with a split-operator Crank-Nicolson approximant [37]. For the real-time propagation with time-dependent $u[n](x, t)$ and $v_{\text{xc}}[n(x, t)]$, the Kohn-Sham equation is nonlinear, and a predictor-corrector scheme is used. We restrict ourselves to spin-neutral systems in this work, so each Kohn-Sham orbital is occupied by a spin-up and a spin-down electron, and the total electron density reads $n(x, t) = 2\sum_{i=1}^{N/2} |\varphi_i(x, t)|^2$.

Figure 2 shows the total energy for the chain with lattice constant $a = 2$ (as used throughout this paper) and $N = 100$ singly charged ions as a function of the shift δ . The total energy is calculated as $E_{\text{total}} = E[\{\varphi_i\}] + E_{\text{ii}}$ with the static ion-ion energy $E_{\text{ii}} = \sum_{i=1}^N \sum_{j<i} [(x_j - x_i)^2 + 1]^{-1/2}$ and the electronic energy $E[\{\varphi_i\}] = T_s[\{\varphi_i\}] + E_{\text{ei}}[n] + U[n] + E_{\text{xc}}[n]$

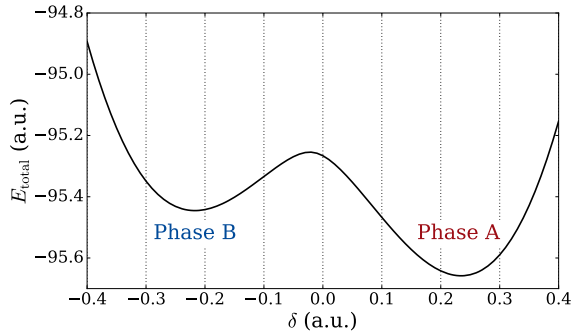


FIG. 2. Total energy for $a = 2$ and $N = 100$ vs shift δ .

where $T_s[\{\varphi_i\}] = -\sum_{i=1}^{N/2} \int dx \varphi_i^*(x) \frac{\partial^2}{\partial x^2} \varphi_i(x)$ is the kinetic energy, $E_{ei}[n] = \int v_{ions}(x)n(x) dx$ is the electron-ion interaction energy, $U[n] = \frac{1}{2} \int u[n](x)n(x) dx$ is the Hartree energy, and $E_{xc}[n] \simeq -\frac{3}{4} \left(\frac{3}{\pi}\right)^{1/3} \int n^{4/3}(x) dx$ is the exchange-correlation energy. There is a global minimum in the phase A ($\delta > 0$) regime at $\delta = 0.235$ and a local minimum in the phase B ($\delta < 0$) at $\delta = -0.217$ [38]. The metallic case $\delta = 0$ is energetically unfavorable (Peierls instability).

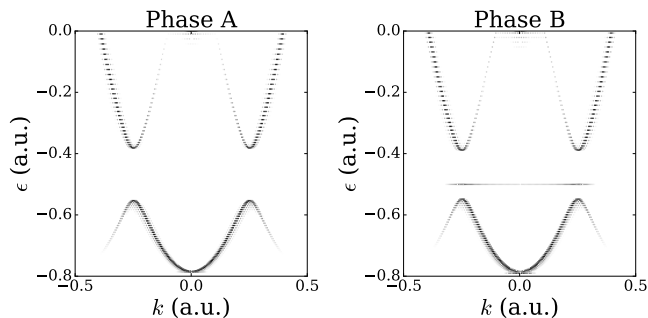


FIG. 3. Band structures of phases A ($\delta = 0.235$) and B ($\delta = -0.217$). The lower band is fully populated. In phase B, one of the two degenerate edge states in the band gap is occupied.

Figure 3 shows the band structures of the two phases at the local minima for $N = 100$. We calculate band structures for finite chains by Fourier-transforming the position-space Kohn-Sham orbitals to k -space [24]. Phase A is an insulator with a completely filled valence band and an unoccupied conduction band. Two edge states are present in the band gap of phase B. They are degenerate and only one of them is occupied. In position space, these states are localized on the edges of the chain, hence the name “edge states.”

The laser pulse used in this work is an $N_{cyc} = 5$ cycle sine-square pulse of frequency $\omega = 0.0075$ (which corresponds to a wavelength of $\simeq 6.1 \mu\text{m}$). The vector potential reads

$$A(t) = A_0 \sin^2 \left(\frac{\omega t}{2N_{cyc}} \right) \sin \omega t \quad (5)$$

for $0 < t < 2\pi N_{cyc}/\omega$ and zero otherwise. The electronic dipole is proportional to

$$X(t) = 2 \sum_{i=1}^{N/2} \int x |\varphi_i(x, t)|^2 dx \quad (6)$$

and recorded during the laser pulse. For some of the cases investigated in this work (e.g. during the transition from phase B to phase A, when the ions are not centered around zero), $X(0) \neq 0$ before the interaction with the laser. To account for this, $X(0)$ is subtracted from $X(t)$ for all t , which only affects the harmonic component at frequency zero. The topological features in the harmonic spectra are qualitatively independent of whether we use the dipole, velocity, current or acceleration to compute the spectra [39, 40].

In order to improve the dynamic range of the harmonic spectra, the dipoles are windowed by a Hann function [41] $w(t) = \sin^2[\pi t/(N_t \Delta t - 1)]$, where N_t is the number of outputs and Δt the output interval. The total dipole strength $D(\omega)$ is then calculated by taking the absolute square of the Fourier transform of the windowed dipole

$$D(\omega) \propto \left| \text{FFT}[w(t)X(t)] \right|^2. \quad (7)$$

III. ROBUSTNESS OF TOPOLOGICAL EFFECTS ON HARMONIC GENERATION

Ref. [28] finds a difference of up to 14 orders of magnitude between harmonic spectra for the two topological phases. The origin of this topological effect is attributed to the destructive interference of all the dipoles of the Kohn-Sham orbitals in phase A due to the completely filled valence band. In contrast, for phase B, destructive interference is imperfect because of the only half-occupied edge states. In the following, the remarkable robustness of that topological effect is illustrated.

A. Size dependence

The harmonic spectra for the two topological phases for $N = 100$ ions and a vector potential amplitude $A_0 = 0.1$ (i.e., an intensity of $\simeq 2 \times 10^{10} \text{ W/cm}^2$) are shown in Fig. 4. The large difference in the harmonic yield observed already in [28] is clearly visible.

In order to investigate how many ions are needed to generate the characteristic spectra of the phases, the number of ions N is decreased. The effect of the chain length on the *high*-harmonic generation is investigated in Ref. [42], although not with a focus on topological effects. Here we focus on the sub-band-gap regime (i.e., harmonic-photon energies are smaller than the band gap of phase A), where the large *qualitative* difference in Fig. 4 is observed. In the sub-band-gap regime, anharmonic intraband motion of the electrons is the origin of

harmonics, and its dependence on the chain length is not obvious. As the many-order-of-magnitude difference between phases A and B is an edge-state effect, one could expect that the ratio of surface (two ions in one dimension) to bulk (the other $N - 2$ ions) is relevant, while *topological* edge-state effects should be independent of N as long as N is large enough to yield an energy spectrum that resembles a band structure. Indeed, increasing N beyond 100 does not qualitatively change the harmonic spectra for both phases.

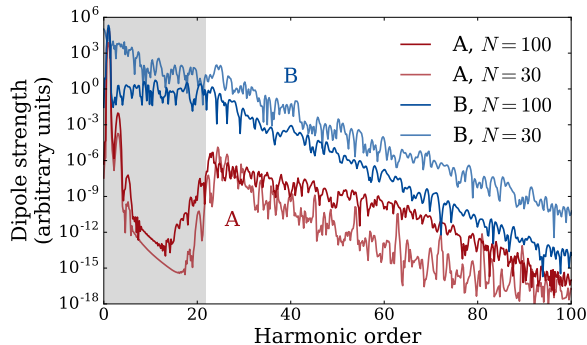


FIG. 4. Harmonic spectra of phases A and B for $N = 100$ and $N = 30$ ions. The gray shade indicates the sub-band-gap regime of phase A.

The harmonic spectra for $N = 30$ are also shown in Fig. 4. Even though there are differences between the harmonic spectra for $N = 100$ and $N = 30$ ions in both phases, the large difference between the phases in the sub-band-gap regime remains qualitatively the same.

Spectra for even smaller N were examined as well. The clear difference between the phases due to perfect and imperfect destructive interference deteriorates only when N is so small ($N < 10$) that no band structure develops. For the extreme case of $N = 2$, the two phases correspond to two diatomic molecules with by 2δ different internuclear distances where the notion of “edge states” does not make sense.

B. Transition between phases

Topological equivalence is often popularly explained as the possibility to continuously deform an object without pinching holes in it or breaking it. Topological difference thus implies the impossibility of such a deformation without changing the topological invariant (e.g., the number of holes in an object). In condensed matter physics, the situation is a bit more complex, as the deformations can be continuous in position space, but the topological invariant changes discontinuously in another, more abstract space. Topological invariants are typically defined for bulk material as winding numbers (e.g., in the space spanned by the 2×2 matrices of a tight-binding Bloch Hamiltonian as a function of lattice momentum k), integrals over the Berry curvature in k -space, or simply

the number of levels below some properly defined zero energy [32, 43, 44].

We can shift continuously from phase B to phase A in position space by increasing the left edge ion’s coordinate x_1 until it pairs up with the right edge ion to form a phase-A chain ($x_1 = x_{N+1} = x_{101}$). Figure 5 shows the orbital energies during the transition for $N = 100$ as well as the edge state orbitals for two exemplary configurations. For each configuration, the self-consistent, stationary electron structure is calculated (i.e., we are not moving the edge ion in real time but use x_1 as an order parameter to describe a hypothetical, adiabatic phase transition).

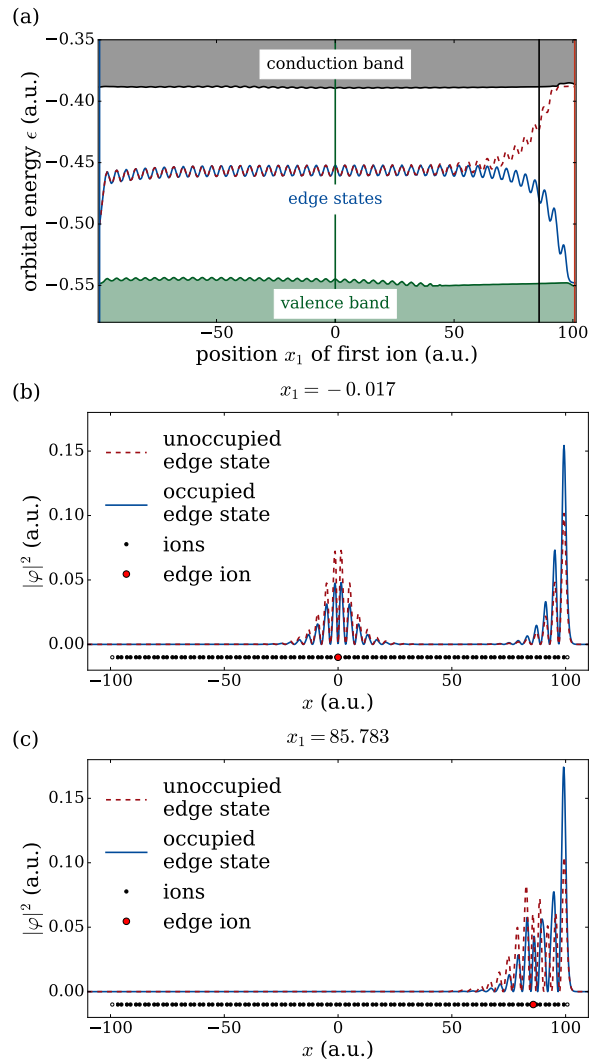


FIG. 5. (a) Orbital energies during the transition from phase B to phase A (vertical lines indicate the positions of the spectra shown in Fig. 6), (b) edge state orbital densities for $x_1 = -0.017$, and (c) $x_1 = 85.783$.

One could expect that the degeneracy of the two edge-state energies is lifted as soon as the inversion symmetry is broken by an $x_1 \neq -x_{100}$. Instead, Fig. 5 shows that the edge-state levels remain degenerate until the edge-

state orbitals start to overlap. For example, for $x_1 \simeq 0$ (when the previously left-edge ion is moved to the center), the two contributions to the edge state orbitals from the right edge and the shifted left-edge ion are still well separated. As a consequence, the energies of the two edge states are still degenerate, just slightly higher than in the original phase-B case. At $x_1 \simeq 86$, the edge states are not degenerate anymore because the contributions on the shifted ion and the right edge overlap significantly. The case $x_1 = 100.783$ almost corresponds to the perfect phase-A case. One of the two degenerate edge states turns into the highest state of the valence band, the other one into the lowest of the conduction band.

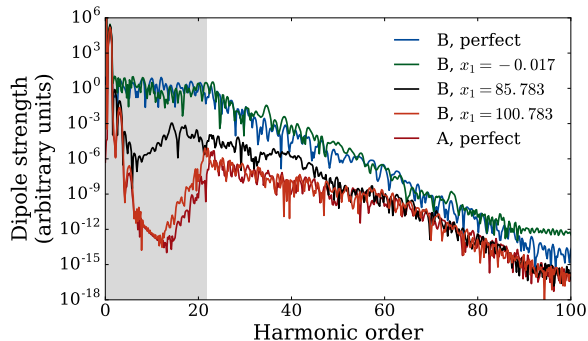


FIG. 6. Harmonic spectra for phase A, phase B, and phase B with $x_1 = -0.017$, $x_1 = 85.7837$, and $x_1 = 100.783$ (these positions are indicated by vertical lines in Fig. 5).

Figure 6 shows harmonic spectra for several x_1 during the transition, as indicated by vertical lines in Fig. 5(a). For $x_1 = -0.017$ the harmonic spectrum is very similar to the pure phase-B case because the band structure did not change qualitatively (the two edge states are still degenerate). For $x_1 = 85.783$, the spectrum already shows a phase-A-like dip, although a smaller one and at lower harmonic order because the energy difference between the two now separated edge states is smaller than the band gap in pure phase A. At $x_1 = 100.783$, the spectrum looks almost like the one for pure phase A. Small deviations are due to the fact that phase B with $x_1 = 100.783$ corresponds to phase A with $\delta = 0.217$ instead of $\delta = 0.235$ (where the total energy is minimal).

C. Disorder in the ion positions

Topological systems with disorder are a topic of current scientific interest (see, e.g., [45, 46]). The role of disorder in harmonic generation has been investigated as well [14]. It has been found that disordered systems generate harmonics at least as well as ordered systems, showing that a band structure is not necessary for efficient harmonic emission from solids.

Disorder is introduced into our model system by randomly shifting the ion positions $x_i \rightarrow x'_i = x'_i + r_i$, mimicking disordered samples or finite temperature. The ran-

dom shifts r_i follow a normal distribution with mean 0 and standard deviation σ_x .

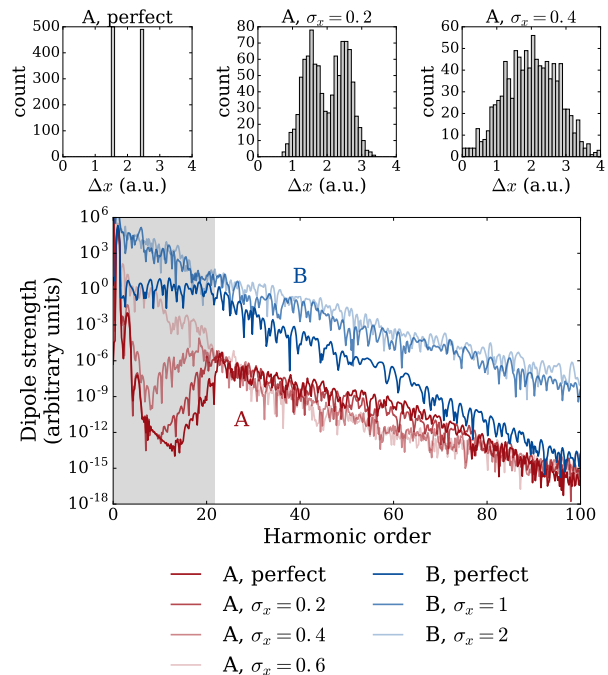


FIG. 7. Top: Histograms of the internuclear distances Δx for phase A with random shifts. Bottom: Harmonic spectra for phases A and B for different standard deviations σ_x .

The harmonic spectra of phases A and B for different standard deviations σ_x and histograms of the internuclear distances are shown in Figure 7. In phase A, the characteristic low harmonic yield below the band gap due to destructive interference of all the dipoles of Kohn-Sham electrons in the valence band disappears with increasing disorder. This is because the bands are “washed out” by disorder, which effectively decreases the band gap. However, the dip in the phase-A spectra survives up to surprisingly high $\sigma_x = 0.4$, where the histogram of the internuclear distances does not show a two-peak distribution of a dimerized chain anymore.

The introduction of random shifts to the ion positions has little impact on the qualitative features of the harmonic spectrum from phase B. This is not surprising because there is no concerted destructive interference to be ruined by disorder in the first place. Therefore, we only show results for extreme disorder $\sigma_x = 1$ and $\sigma_x = 2$. For such high values, many of the random shifts are already on the order of the lattice constant $a = 2$, i.e., ions are swapped. These spectra are thus examples for harmonic generation from purely random linear chains.

D. Disorder in the ion potentials

Another way of introducing disorder is to randomly vary the smoothing parameters ε_i in the Coulomb po-

tentials $v_i(x) = -[(x - x_i)^2 + \varepsilon_i]^{-1/2}$ of the ions, which affects the depth of the potential. One may view this as randomly changing the local ionization potentials of the atoms that constitute the chain. The ε_i follow a normal distribution with mean 1 and standard deviation σ_ε . If a random ε_i happens to be < 0 , it is set to 0.

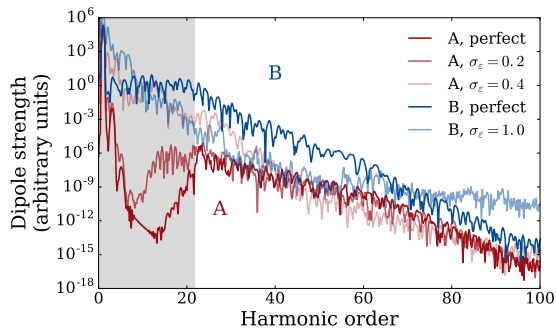


FIG. 8. Harmonic spectra of phases A and B for different standard deviations σ_ε .

The harmonic spectra of phases A and B for different standard deviations σ_ε are shown in Figure 8. In phase A, there are no large deviations in the above-band-gap regime (white background). In the sub-band-gap regime, the characteristic low-harmonic yield disappears only for surprisingly large random variations (similar to the case of disordered ion positions in the previous subsection).

IV. SUMMARY

Harmonic generation in different topological phases was investigated using a linear chain as a model system.

The harmonic yield was calculated with time-dependent density functional theory, taking the response of all electrons to the laser field into account. The previously found low harmonic yield of phase A (without topological edge states) compared to phase B (with topological edge states) in the sub-band-gap regime was confirmed, and the robustness of this many-order-of-magnitude topological effect was studied with respect to (i) the size of the chain, (ii) a continuous transition between the two topological phases, and (iii) disorder. When the number of ions N in the system was lowered, both phases retained the characteristic features of their harmonic spectra down to very low $N \simeq 10$. During the continuous transition from phase B to phase A by moving one of the edge ions to the other side, the degeneracy of the edge states and the harmonic spectrum remained of phase-B character until the shifted ion paired up with the opposite edge ion. Random shifts of the ions and changes in the ionic potentials of the ions had to be surprisingly large in order to destroy the characteristic features of the harmonic spectra of both phases.

Regarding possible applications, robustness is probably the most important and striking asset of topological effects. Hence, it may be argued that the observed robustness in the present paper is not surprising. However, it is important to point out that we observe this robustness for a time-dependent density-functional model of a strongly driven finite chain for which the topological invariant of the bulk Su-Schrieffer-Heeger chain does not exist.

ACKNOWLEDGMENTS

Inspiring discussions with Alexander Szameit are gratefully acknowledged.

-
- [1] Martin Schultze, Krupa Ramasesha, C.D. Pemmaraju, S.A. Sato, D. Whitmore, A. Gandman, James S. Prell, L. J. Borja, D. Prendergast, K. Yabana, Daniel M. Neumarck, and Stephen R. Leone, “Attosecond band-gap dynamics in silicon,” *Science* **346**, 1348–1352 (2014).
 - [2] M. Lucchini, S. A. Sato, A. Ludwig, J. Herrmann, M. Volkov, L. Kasmi, Y. Shinohara, K. Yabana, L. Gallmann, and U. Keller, “Attosecond dynamical Franz-Keldysh effect in polycrystalline diamond,” *Science* **353**, 916–919 (2016).
 - [3] M. Th Hassan, T. T. Luu, A. Moulet, O. Raskazovskaya, P. Zhokhov, M. Garg, N. Karpowicz, A. M. Zheltikov, V. Pervak, F. Krausz, and E. Goulielmakis, “Optical attosecond pulses and tracking the nonlinear response of bound electrons,” *Nature* **530**, 66–70 (2016).
 - [4] A. Sommer, E. M. Bothschafter, S. A. Sato, C. Jakubeit, T. Latka, O. Razskazovskaya, H. Fattahi, M. Jobst, W. Schweinberger, V. Shirvanyan, V. S. Yakovlev, R. Kienberger, K. Yabana, N. Karpowicz, M. Schultze, and F. Krausz, “Attosecond nonlinear polarization and light-matter energy transfer in solids,” *Nature* **534**, 86–90 (2016).
 - [5] Shambhu Ghimire, Anthony D. DiChiara, Emily Sistrunk, Pierre Agostini, Louis F. DiMauro, and David A. Reis, “Observation of high-order harmonic generation in a bulk crystal,” *Nat Phys* **7**, 138–141 (2011).
 - [6] O. Schubert, M. Hohenleutner, F. Langer, B. Urbanek, C. Lange, U. Huttner, D. Golde, T. Meier, M. Kira, S.W. Koch, and R. Huber, “Sub-cycle control of terahertz high-harmonic generation by dynamical Bloch oscillations,” *Nat Photon* **8**, 119–123 (2014).
 - [7] M. Hohenleutner, F. Langer, O. Schubert, M. Knorr, U. Huttner, S. W. Koch, M. Kira, and R. Huber, “Real-time observation of interfering crystal electrons in high-harmonic generation,” *Nature* **523**, 572–575 (2015).
 - [8] G. Vampa, T. J. Hammond, N. Thiré, B. E. Schmidt, F. Légaré, C. R. McDonald, T. Brabec, D. D. Klug, and P. B. Corkum, “All-optical reconstruction of crystal band structure,” *Phys. Rev. Lett.* **115**, 193603 (2015).

- [9] T. T. Luu, M. Garg, S. Yu Kruchinin, A. Moulet, M. Th Hassan, and E. Goulielmakis, “Extreme ultraviolet high-harmonic spectroscopy of solids,” *Nature* **521**, 498–502 (2015).
- [10] F. Langer, M. Hohenleutner, U. Huttner, S.W. Koch, M. Kira, and R. Huber, “Symmetry-controlled temporal structure of high-harmonic carrier fields from a bulk crystal,” *Nat Photon* **11**, 227–231 (2017).
- [11] Nicolas Tancogne-Dejean, Oliver D. Mücke, Franz X. Kärtner, and Angel Rubio, “Impact of the electronic band structure in high-harmonic generation spectra of solids,” *Phys. Rev. Lett.* **118**, 087403 (2017).
- [12] G. Vampa, T. J. Hammond, M. Taucer, Xiaoyan Ding, X. Ropagnol, T. Ozaki, S. Delprat, M. Chaker, N. Thiré, B. E. Schmidt, F. Légaré, D. D. Klug, A. Yu Naumov, D. M. Villeneuve, A. Staudte, and P. B. Corkum, “Strong-field optoelectronics in solids,” *Nature Photonics* **12**, 465–468 (2018).
- [13] M. Garg, H. Y. Kim, and E. Goulielmakis, “Ultimate waveform reproducibility of extreme-ultraviolet pulses by high-harmonic generation in quartz,” *Nature Photonics* **12**, 291–296 (2018).
- [14] Yong Sing You, Yanchun Yin, Yi Wu, Andrew Chew, Xiaoming Ren, Fengjiang Zhuang, Shima Gholam-Mirzaei, Michael Chini, Zenghu Chang, and Shambhu Ghimire, “High-harmonic generation in amorphous solids,” *Nature Communications* **8**, 724 (2017).
- [15] Georges Ndabashimiye, Shambhu Ghimire, Mengxi Wu, Dana A. Browne, Kenneth J. Schafer, Mette B. Gaarde, and David A. Reis, “Solid-state harmonics beyond the atomic limit,” *Nature* **534**, 520–523 (2016).
- [16] Takuya Higuchi, Christian Heide, Konrad Ullmann, Heiko B. Weber, and Peter Hommelhoff, “Light-field-driven currents in graphene,” *Nature* **550**, 224 EP – (2017).
- [17] Matthias Baudisch, Andrea Marini, Joel D. Cox, Tony Zhu, Francisco Silva, Stephan Teichmann, Mathieu Mascotte, Frank Koppens, Leonid S. Levitov, F. Javier García de Abajo, and Jens Biegert, “Ultrafast nonlinear optical response of dirac fermions in graphene,” *Nature Communications* **9**, 1018 (2018).
- [18] Christian Heide, Takuya Higuchi, Heiko B. Weber, and Peter Hommelhoff, “Coherent electron trajectory control in graphene,” *Phys. Rev. Lett.* **121**, 207401 (2018).
- [19] G. P. Zhang, M. S. Si, M. Murakami, Y. H. Bai, and Thomas F. George, “Generating high-order optical and spin harmonics from ferromagnetic monolayers,” *Nature Communications* **9**, 3031 (2018).
- [20] Paul B. Corkum, “Plasma perspective on strong field multiphoton ionization,” *Physical Review Letters* **71**, 1994–1997.
- [21] M. Lewenstein, Ph. Balcou, M. Yu. Ivanov, Anne L’Huillier, and P. B. Corkum, “Theory of high-harmonic generation by low-frequency laser fields,” *Phys. Rev. A* **49**, 2117–2132 (1994).
- [22] G. Vampa and T. Brabec, “Merge of high harmonic generation from gases and solids and its implications for attosecond science,” *Journal of Physics B: Atomic, Molecular and Optical Physics* **50**, 083001 (2017).
- [23] Mengxi Wu, Dana A. Browne, Kenneth J. Schafer, and Mette B. Gaarde, “Multilevel perspective on high-order harmonic generation in solids,” *Phys. Rev. A* **94**, 063403 (2016).
- [24] Kenneth K. Hansen, Tobias Deffge, and Dieter Bauer, “High-order harmonic generation in solid slabs beyond the single-active-electron approximation,” *Phys. Rev. A* **96**, 053418 (2017).
- [25] Hui Zhai, Mikael Rechtsman, Yuan-Ming Lu, and Kun Yang, “Focus on topological physics: from condensed matter to cold atoms and optics,” *New Journal of Physics* **18**, 080201 (2016).
- [26] Hamed Koochaki Kelardeh, Vadym Apalkov, and Mark I. Stockman, “Graphene superlattices in strong circularly polarized fields: Chirality, Berry phase, and attosecond dynamics,” *Phys. Rev. B* **96**, 075409 (2017).
- [27] Tran Trung Luu and Hans Jakob Wörner, “Measurement of the Berry curvature of solids using high-harmonic spectroscopy,” *Nature Communications* **9**, 916 (2018).
- [28] Dieter Bauer and Kenneth K. Hansen, “High-harmonic generation in solids with and without topological edge states,” *Phys. Rev. Lett.* **120**, 177401 (2018).
- [29] R. E. F. Silva, Jimnez-Galn, B. Amorim, O. Smirnova, and M. Ivanov, “Topological strong field physics on sub-laser cycle time scale,” arXiv:1806.11232v2 [cond-mat, physics:physics] .
- [30] Alexis Chacón, Wei Zhu, Shane P. Kelly, Alexandre Dauphin, Emilio Pisanty, Antonio Picón, Christopher Ticknor, Marcelo F. Ciappina, Avadh Saxena, and Maciej Lewenstein, “Observing topological phase transitions with high harmonic generation,” arXiv:1807.01616 [cond-mat, physics:quant-ph] .
- [31] W. P. Su, J. R. Schrieffer, and A. J. Heeger, “Solitons in polyacetylene,” *Phys. Rev. Lett.* **42**, 1698–1701 (1979).
- [32] J.K. Asbóth, L. Oroszlány, and A. Pályi, *A Short Course on Topological Insulators*, Lecture Notes in Physics, Vol. 919 (Springer, 2016).
- [33] Erich Runge and E. K. U. Gross, “Density-functional theory for time-dependent systems,” *Physical Review Letters* **52**, 997–1000.
- [34] C. A. Ullrich, *Time-Dependent Density-Functional Theory: Concepts and Applications* (Oxford University Press, Oxford, 2011).
- [35] Ady Stern and Netanel H. Lindner, “Topological quantum computation—from basic concepts to first experiments,” *Science* **339**, 1179 (2013).
- [36] Valla Fatemi, Sanfeng Wu, Yuan Cao, Landry Bretheau, Quinn D. Gibson, Kenji Watanabe, Takashi Taniguchi, Robert J. Cava, and Pablo Jarillo-Herrero, “Electrically tunable low-density superconductivity in a monolayer topological insulator,” *Science* **362**, 926 (2018).
- [37] Dieter Bauer, ed., *Computational Strong-Field Quantum Dynamics* (DeGruyter, Berlin, 2017).
- [38] Figure 2 corrects panel (a) of Fig. 1 in [28] (which, however, does not affect any of the other results and the conclusions in [28]).
- [39] A. D. Bandrauk, S. Chelkowski, D. J. Diestler, J. Manz, and K.-J. Yuan, “Quantum simulation of high-order harmonic spectra of the hydrogen atom,” *Physical Review A* **79**, 023403.
- [40] Jan Conrad Baggesen and Lars Bojer Madsen, “On the dipole, velocity and acceleration forms in high-order harmonic generation from a single atom or molecule,” *Journal of Physics B: Atomic, Molecular and Optical Physics* **44**, 115601.
- [41] F. J. Harris, “On the use of windows for harmonic analysis with the discrete Fourier transform,” *Proceedings of the IEEE* **66**, 51–83 (1978).

- [42] Kenneth K. Hansen, Dieter Bauer, and Lars Bojer Madsen, “Finite-system effects on high-order harmonic generation: From atoms to solids,” *Phys. Rev. A* **97**, 043424 (2018).
- [43] M. Z. Hasan and C. L. Kane, “Colloquium,” *Rev. Mod. Phys.* **82**, 3045–3067 (2010).
- [44] Marcel Franz and Laurens Molenkamp, eds., *Topological Insulators*, Contemporary Concepts of Condensed Matter Science, Vol. 6 (Elsevier, 2013).
- [45] Cenke Xu and J. E. Moore, “Stability of the quantum spin hall effect: Effects of interactions, disorder, and \mathbb{Z}_2 topology,” *Physical Review B* **73**, 045322.
- [46] Simon Stützer, Yonatan Plotnik, Yaakov Lumer, Paraj Titum, Netanel H. Lindner, Mordechai Segev, Mikael C. Rechtsman, and Alexander Szameit, “Photonic topological anderson insulators,” *Nature* **560**, 461–465 (2018).